DOI: 10.13009/EUCASS2019-200

Experiments on Görtler vortices of controllable intensity in a hypersonic compression corner flow

P.V. Chuvakhov[*ab], *V.N. Radchenko*[**b] *and E.A. Alexandrova*[***b]

[a]*Central Aerohydrodynamic Institute (TsAGI), 1 Zhukovskogo Str., Zhukovsky, 140180, Russia*
[b]*Moscow Institute of Physics and Technology (MIPT), 9 Institutskiy Per., Dolgopridny, 141701, Russia*
[*] pavel_chuvakhov@mail.ru
[**] vradchenko61@gmail.com
[***] miptjane@gmail.com

Abstract

Controlled experiments on heat transfer are carried out in shock wind tunnel UT-1M (TsAGI) for Mach 8 15° compression corner flow affected by Goertler vortices. Experiments are focused on the Reynolds number $Re_{\infty,L}=(1.75\pm0.09)\times10^5$ based on the sharp flat plate length at which the reattachment flow is close to laminar. The effect of streamwise vortices of different intensity on mean level of heat flux and its variation at the reattachment region is investigated. Intensity of the vortices is varied by variation of the height of spanwise rake of cylindrical pins (seeding elements) placed on the plate ahead of the separation bubble.

1. Introduction

Design of heat protection systems for control surfaces of aerospace vehicles (elevons, flaps) raises a fundamental problem of supersonic compression corner flow. Flow reattachment gives rise to excessive heat flux regions and form favorable conditions for Goertler vortices to occur. Such vortices are mainly seeded by irregularities of the surface that also determine the intensity of the vortices. Being amplified in the reattachment region, the vortices result in considerable variations of heat flux with amplitudes up to 100% of its spanwise-averaged value (see, e.g., [1]). The presence of vortices also leads to increased mean value of heat flux, which is commonly connected to transitional state of the reattachment flow [2]. However, numerical investigations [1, 3] show that this may happen in a purely laminar flow. Though different in nature, similar effect was observed in direct numerical simulation [4] of fundamental breakdown on Mach 6 cone where regular streamwise streaks occurred because of nonlinear processes and caused sharp increase of heat flux before the transition to turbulence took over.

The purpose of the present study is to support numerical findings of [1, 3] experimentally, thereby revealing the effect of the Goertler vortices intensity on the mean level and variations of heat flux in the reattachment region. To this effect, the vortices are seeded ahead of the separation bubble by a spanwise rake of cylindrical roughness elements of same height. Varying the height allows to change the intensity of the vortices.

2. Experimental setup and measuring technique

The test model is a flat plate of 320×150 mm shown in Fig. 1 with a 15° wedge installed on the top. The plate consists of the fiberglass insert 1 flash mounted into a steel frame. The wedge (ramp) is a strait triangular prism of steel with the insert 2 of Plexiglas. A part of the wedge surface subjected to flow is 150 mm long. The sidewalls are designed both for the plate and for the wedge to minimize side effects thereby preserving nominally two-dimensional base flow.

The hinge line is located at L=50 mm apart from the exchangeable sharp leading edge (see fig. 2a; the edge thickness is 21±1 μm). The streamwise length of the leading edge element is 27 mm. It connects tightly with the plate frame to form a single plane. The possible imperfection of the connection is uniform in spanwise direction and is designed to be an upward-facing step with less than 10μm height. Such step is at the bottom of the boundary layer for the present experiments and does not affect the flow, because the corresponding value of Re_{kk} for the step is well under 25 [5].

DOI: 10.13009/EUCASS2019-200

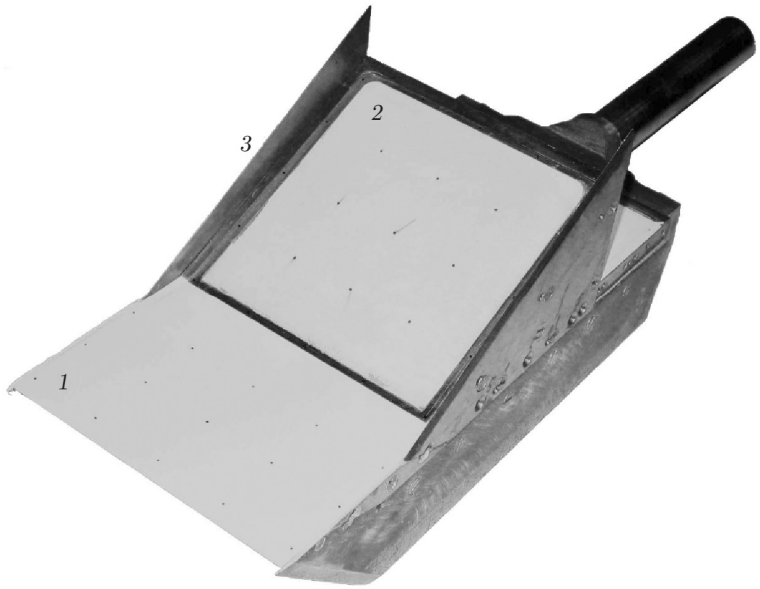

Figure 1: Experimental mode:
1 – flat plate of fiberglass; 2 – wedge with thermal insulating insert of Plexiglas; 3 – sidewalls.

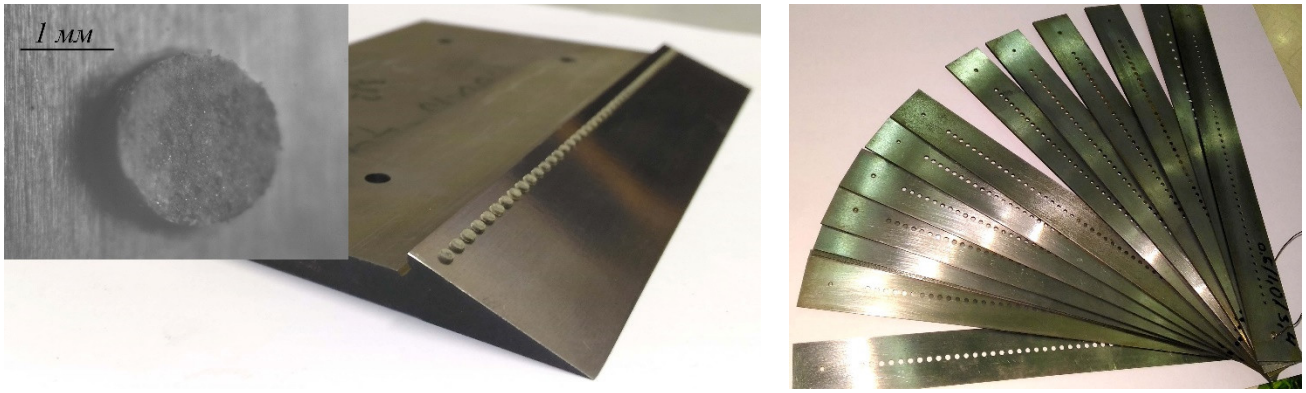

(a) (b)

Figure 2: a) Example of roughness on the leading edge element (x_k=23.5 mm for present picture only); enlarged roughness element under the microscope; b) templates for roughness formation.

Intensity of the vortices is varied in experiments by changing the intensity of steady disturbances ahead of the separation bubble. The disturbances develops behind a rake of cylindrical roughness elements distributed periodically in spanwise direction at l_k=17 mm apart from the leading edge (Fig. 2a). The diameter of the roughness element is 1.7±0.1 mm, the spacing is 3.4±0.1 mm. The roughness is formed by using specially designed steel templates of thickness from 0.1 to 1.6 mm (Fig. 1b) with two-component polyester solidifying composition that is put onto the metal surface of the leading edge through the templates. There are six sharp leading edges manufactured and polished, with the surface roughness measured within 0.8 μm and the edge thickness of 21±1 μm.

Experiments are conducted in the shock wind tunnel UT-1M (TsAGI) at Mach number 8, stagnation temperature T_0≈735±5 K and total pressure p_0=15.3±0.7 bar. Corresponding unit Reynolds number is $\mathrm{Re}_{\infty,1}=(3.505\pm0.168)\times10^6$ m^{-1}, which gives the value $\mathrm{Re}_{\infty,L}=(1.75\pm0.09)\times10^5$ based on the hinge line station L=50 mm. The chosen parameters correspond to the laminar state of flow at reattachment region according to the criterion of [6]: $\mathrm{Re}_{\infty,L}<5\times10^5$.

The wind tunnel operates in Ludwig scheme. A lengthy heated high-pressure channel is followed by the Mach 8 profiled nozzle with the exit diameter of 500 mm. A single run duration is about 40 ms, for which the flow has nearly constant characteristics in the test chamber. An example of evolution of stagnation parameters is present in Fig. 3.

Thermal effect of vortices is determined using panoramic patterns of heat flux over the flat plate and wedge surfaces covered with thermal insulating material (over the inserts of fiberglass or Plexiglas). Such patterns are resulted from the thermal measurements of a surface temperature rise during a run by making use of temperature sensitive paints

DOI: 10.13009/EUCASS2019-200

(TSP) developed in TsAGI. With known measurement timing, properties of thermal insulating inserts (items 1 and 2 in Fig. 1), wall temperature and flow conditions, one can derive a heat flux from the flow to the surface and express it in the form of dimensionless heat flux coefficient hereafter referred to as Stanton number, St [7]:

$$\mathrm{St} = \frac{q_w}{\rho_\infty u_\infty c_p \left(T_0 - T_w\right)} = \frac{\mu_w/\mu_\infty}{\mathrm{Pr}\cdot \mathrm{Re}_{\infty,1}} \frac{1}{T_0 - T_w} \times \frac{dT}{d\bar{n}} . \quad (1)$$

Repeatability of experiments was confirmed by doing several experiments again on different days and with remade roughness rakes.

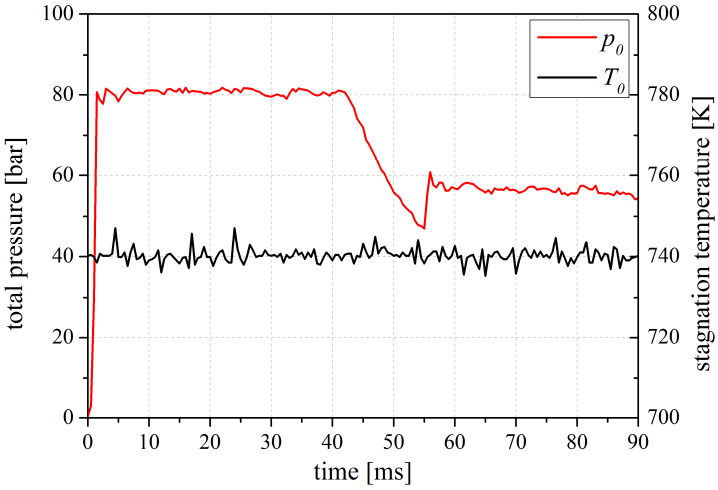

Figure 3: Example of time evolution of total pressure p_0 and stagnation temperature T_0 during a single run of wind tunnel.

3. Results

3.1 Schlieren visualization

Figure 4 illustrates the flow patterns in the presence of roughness rake of different height. In case of no roughness, the pattern is usual for hypersonic compression corner flow (Fig. 4a). There is a bow shock wave generated by viscous interaction near the plate leading edge. A light curve near the surface marks the boundary layer development, starting at the leading edge and follows downstream. The curve deviates from the surface ahead of the hinge (corner) line, which marks the station of the boundary layer separation. Passing over the separation bubble, the curve comes back to the wedge surface at the station of the boundary layer reattachment. Maximum heat flux is observed near the thinnest part between the curve and the wedge surface that is commonly called a 'neck. It is not straightforward how to measure the neck station, though its approximate value is $x_{\mathrm{neck}}\approx$30 mm for the cases k=0.0 mm and 0.6 mm (Fig. 4a and b). Separation and reattachment of flow produce the corresponding shock waves that propagate downstream, combine and interact with the bow shock wave forming the complicated flow pattern. There remains a hardly visible rest of the bow shock wave (Fig. 4a) downstream the waves interaction that falls onto the surface near the station x=71 mm measured from the hinge line. This station will be reminded for analysis of TSP results.

One may note two features relative for laminar separated flow: 1) separation bubble is rather lengthy and its outer edge is inclined at small angle with respect to the plate surface; 2) the boundary layer curve is distinct behind the reattachment. This may point to the fact that the observed flow is laminar downstream the reattachment.

Adding the roughness rake of heights k<0.6 mm does not affect the separated flow and only adds a shock wave from the roughness elements. The further increase of the height leads to slight increase of separation bubble (see Fig. 4b). This might be caused by entropy layer effect that appears due to roughness penetrated into the supersonic part of the boundary layer. Similar effect was observed previously in both numerical and experimental investigations of compression corner flow behind blunt leading edge that produced the entropy layer (see e.g. [1] for details and additional references). The roughness makes the reattached boundary layer thicker and smoothen the Schlieren images, which could point to earlier turbulization of the flow.

DOI: 10.13009/EUCASS2019-200

The tallest roughness rake of k=1.2 mm (Fig. 4c) protrudes to the edge of the hypersonic boundary layer. This leads to reduction of the separated bubble size. Thus,the separation zone elongates for small roughness heights and shrinks for large ones. The observed reversal trend is also relevant to the entropy layer effect. Visible is a small separation region in front of the roughness rake. The roughness-induced shock wave interacts with the bow shock wave and pushes it aside of the surface. The flow is highly disturbed in presence of tall roughness rake. The flow features becomes highly smoothened behind the reattachment.

One may note that the roughness rake placed at 17 mm downstream the leading edge does not affect the separation station. Additional experiments with the roughness placed at 23.5 mm showed that separation became sensitive to the roughness height, especially for higher Reynolds number cases, when the separation occurred at roughness station.

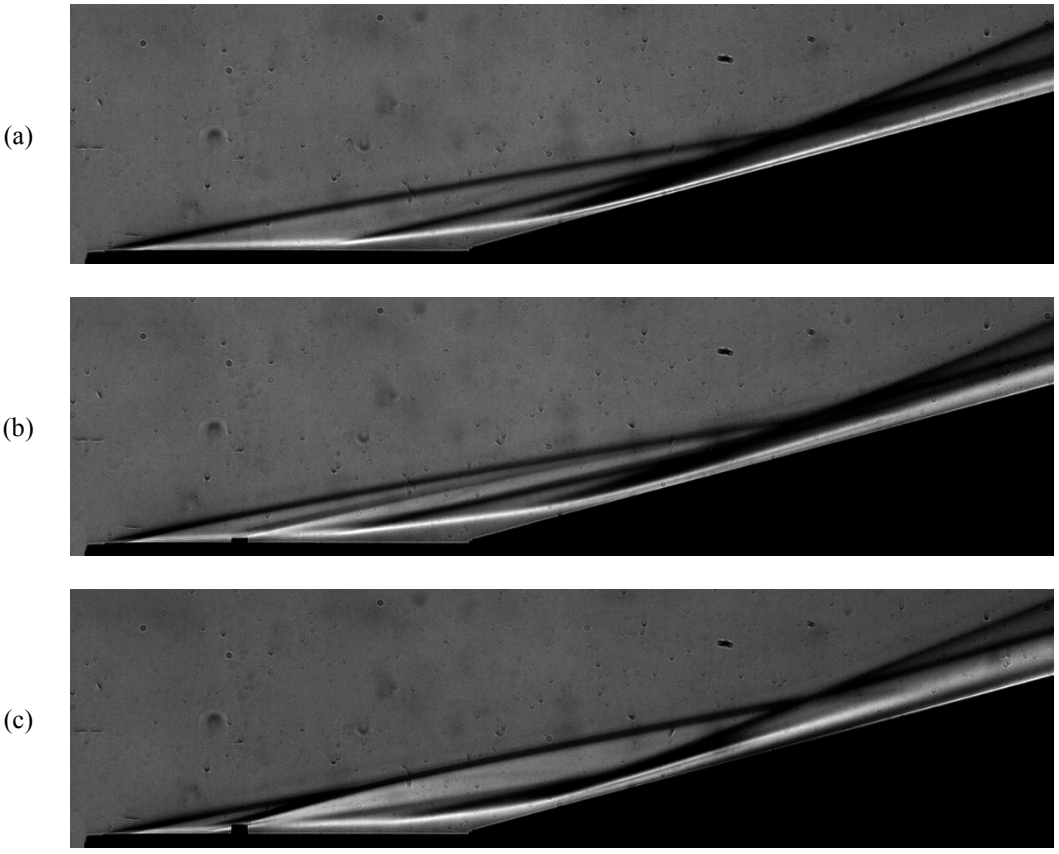

Figure 4: Schlieren visualization of flow in compression corner with a roughness rake of height k=*0.0* (a); 0.6 (b); 1.2 mm (c).

3.2 Thermal patterns

Figure 5 shows the distribution of St over the model surface at two different roughness heights: k = 0 mm (Fig. 5a, no roughness) and k = 0.6 mm (Fig. 5b). The coordinates are plotted with respect to the hinge line that is 50 mm downstream from the leading edge. All experiments are done at low Reynolds numbers, which suggests laminar reattachment flow in accord to the criterion [6]. Figure 5a partially confirms this: heat flux increases by the end of the wedge, which seems to correspond to the laminar-turbulent transition process. Note that the weak bow shock wave reaches the surface at x≈71 mm (see above discussion on Fig. 4a), which may trigger or somehow affect the transition.

Despite the absence of roughness rake (Fig.5a), the reattachment flow is subjected to Goertler-type vortices that occur without being artificially excited. The spanwise variation of St due to vortices attain maximum on the dashed line behind both the reattachment and the neck. This station does not coincide with the local maximum of spanwise-averaged St distribution (black solid line). The two lines becomes closer as the roughness height increases, with the dashed line being always from the left.

Figure 6a illustrates z-averaged (spanwise-averaged) $St_{zAvg}(x)$ distribution that slowly rises downstream the reattachment station. This should be attributed to the combined effect of vortices and possible transition, because the latter cannot be excluded based on the available data. Note that St_{zAvg} attains maximum near x_{max}≈60 mm and then

DOI: 10.13009/EUCASS2019-200

begins decreasing, which is accompanied by noticeable attenuation of thermal footprint of vortices (Fig. 5a). Nevertheless, St_{zAvg} begins increasing again at x≈75 mm, which points to the fact that regular streamwise vortices added more to heat flux in comparison with transition process for x<75 mm. This description should remain valid in purely laminar flow behind the reattachment. Therefore, the vortices themselves are able to increase the average heat transfer even if the flow is laminar. It is to be noted that the maximum of $St_{zAvg}(x_{max})$ is poorly expressed, though its station Reynolds number with respect to the hinge line, $Re_{\infty,1}\times x_{max}$, correlates well with those observed in different wind tunnels at M=8 [8] and M=7.7 [9].

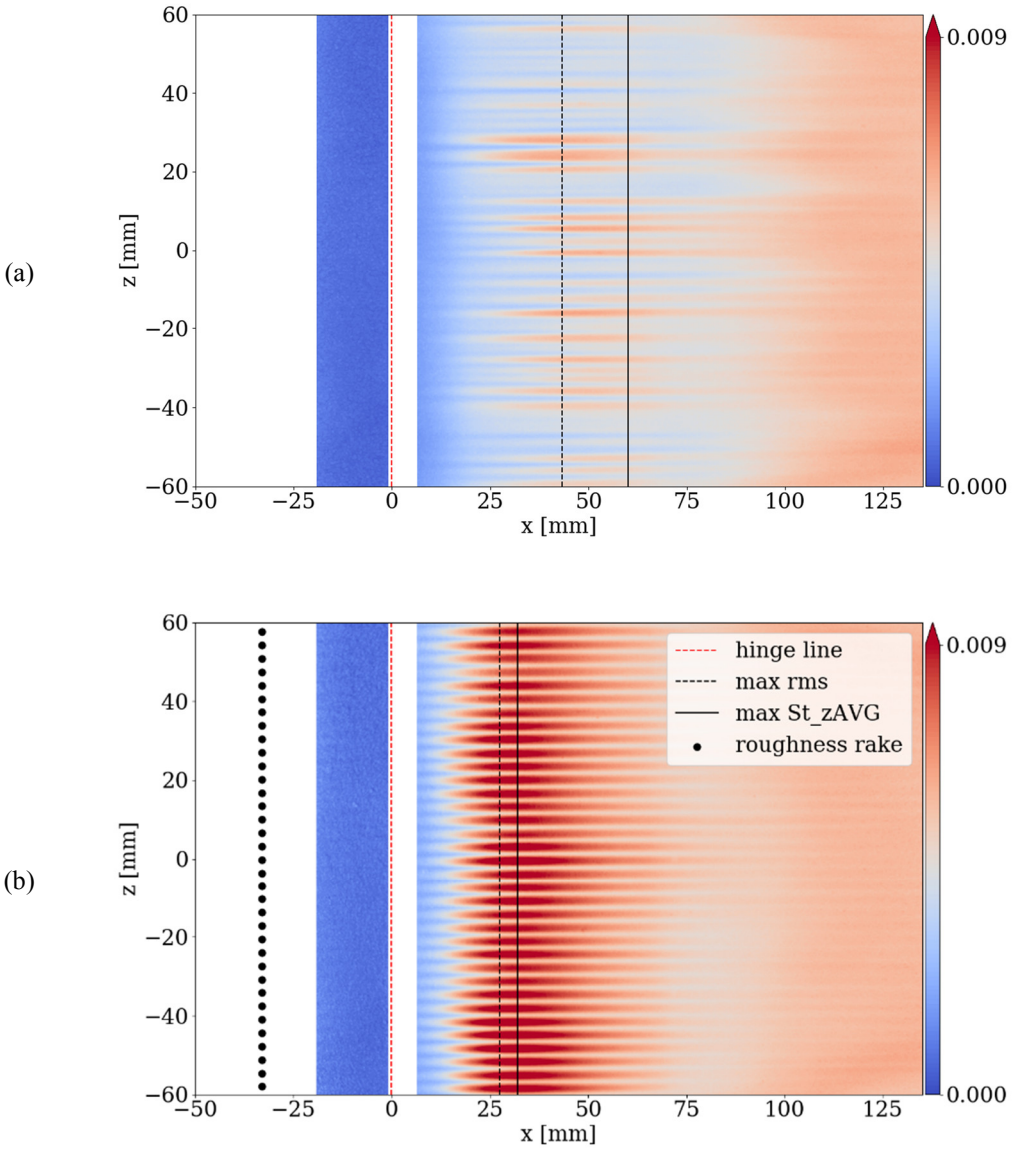

Figure 5: Example distributions of St for k=0 (a) and 0.6 mm (b); view from the top.
Leading edge corresponds to x_{LE}=-50mm. Roughness rake is not precise scale. Max lines correspond to maximum stations of either St_{zAvg} or its rms deviations.

The above conclusion becomes more evident in the presence of the roughness rake, when the vortices are stronger than those induced naturally (see Fig. 5b and 6b). The maximum of St_{zAvg} is now very close to the neck station is well above the value for no roughness case. Again, the vortices quickly disappear downstream with more rapid reduction of St_{zAvg} until the station x≈75 mm, when the behavior of $St_{zAvg}(x)$ becomes quite similar to that for no roughness case (cf. Fig. 6a and 6b). In particular, this gives rise to very close (possibly turbulent) St levels by the end of the plate. Note the slight hump at x≈60 mm that presumably correspond to the fall of the weak bow shock.

The spanwise structure of vortices is illustrated in Fig. 5 and 7. It is rather chaotic for low heights of the roughness rake (Fig. 5a and 7a, k=0.0 mm) and changes when the sharp leading edge is polished or replaced (not shown here).

DOI: 10.13009/EUCASS2019-200

The structure becomes regular following the location of the roughness elements only for $k > 0.4$ mm (see e.g. Fig. 5b and 7b, k=0.6 mm).

It is also to be noted that a thermally visible part of the flat plate on the right hand of the hinge line (the red dashed line of Fig. 5) is inside the separation bubble. The vortices are not visible there in thermal patterns, but the poor imprint of the roughness rake disturbances is present in Fig. 5b.

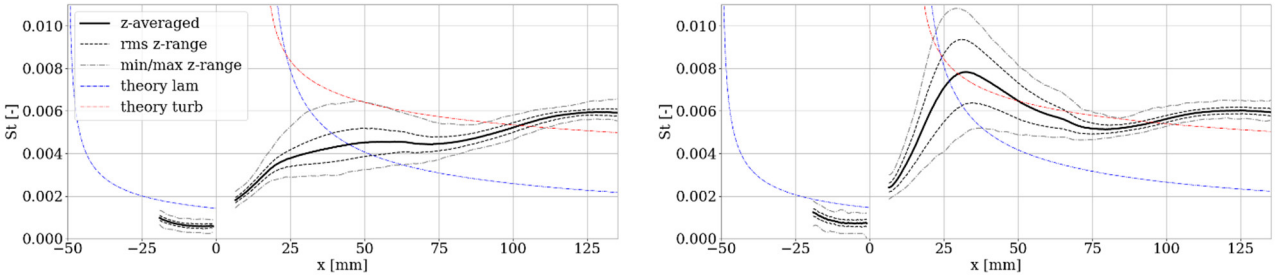

(a) (b)

Figure 6: Spanwise-averaged $St_{zAvg}(x)$ distribution with rms and min/max spanwise deviations due to vortices. Subfigures (a) and (b) correspond to those of Figure 5. See Eq. (4) of next section for definition of flat plate/wedge theory curves.

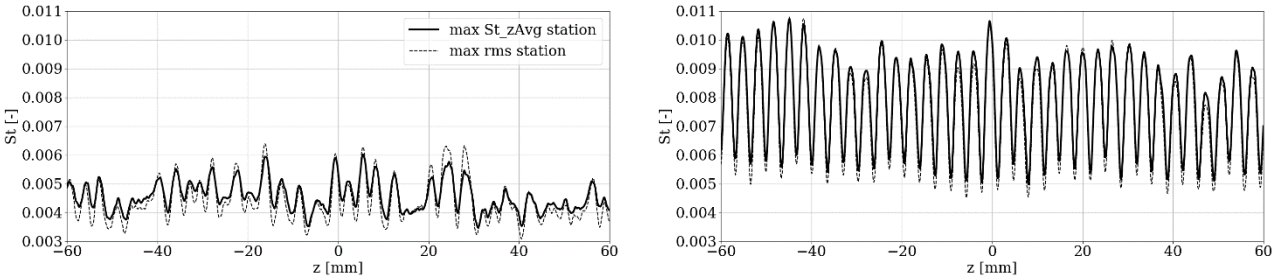

(a) (b)

Figure 7: Spanwise distribution $St(x_{max},z)$; x_{max} corresponds to the maximum station of either $St_{zAvg}(x)$ or its rms deviations. Subfigures (a) and (b) correspond to those of Figure 5.

3.3 Data reduction

Laminar boundary layer thickness over a sharp flat plate is evaluated as Ginoux [10]:

$$\frac{\delta}{x}\sqrt{\frac{\mathrm{Re}_{e,x}}{C^*}} = K + 2.21\frac{\gamma-1}{2}M_e^2 + 1.93\frac{T_w - T_{ad}}{T_e}, \qquad C^* = \frac{\mu^* T_e}{\mu_e T^*} \tag{2}$$

where K=5 for boundary layer thickness at u=0.99U_e, while K=1.72 for the displacement thickness, and C^* is a Chapman–Rubesin constant based on Eckert's reference temperature T^*=0.28T_e+0.50T_w+0.22T_r. Recovery temperature is defined as T_r=T_e×(1+0.5r(γ-1)M_e^2), with r=$Pr^{0.5}$ for laminar boundary layer. Dynamic coefficient of viscosity is computed in accord with Sutherland's law:

$$\frac{\mu(T)}{\mu_{ref}} = \frac{T_{suth} + T_{ref}}{T_{suth} + T}\left(\frac{T}{T_{ref}}\right)^{1.5}, \tag{3}$$

DOI: 10.13009/EUCASS2019-200

where T_{ref}=273.11 K, μ_{ref}=1.716×10^{-5} kg/(m·s), T_{suth}=*110.4* K.

Figure 8a shows self-similar profiles *u(η), T(η)* that have been obtained numerically by solving compressible boundary layer equations for M_∞=8, T_0=*735 K*, T_w=*293 K*, Pr=0.72. Physical coordinates are recovered from the inner coordinate as $y=\eta x(Re_{e,x})^{-0.5}$. Figure 8b illustrates the corresponding values of $Re_{kk}=\rho_k u_k k/\mu_k$ for all the experiments under consideration. For x_k=17 mm, the viscous interaction parameter $\chi=M^3(C/Re_{\infty,xk})^{0.5}$ is 1.6 which is not small to readily neglect the viscous-invscid interaction at the roughness station. However, weak viscous-inviscid interaction is a good approximation to use for the reduction of the present experiments.

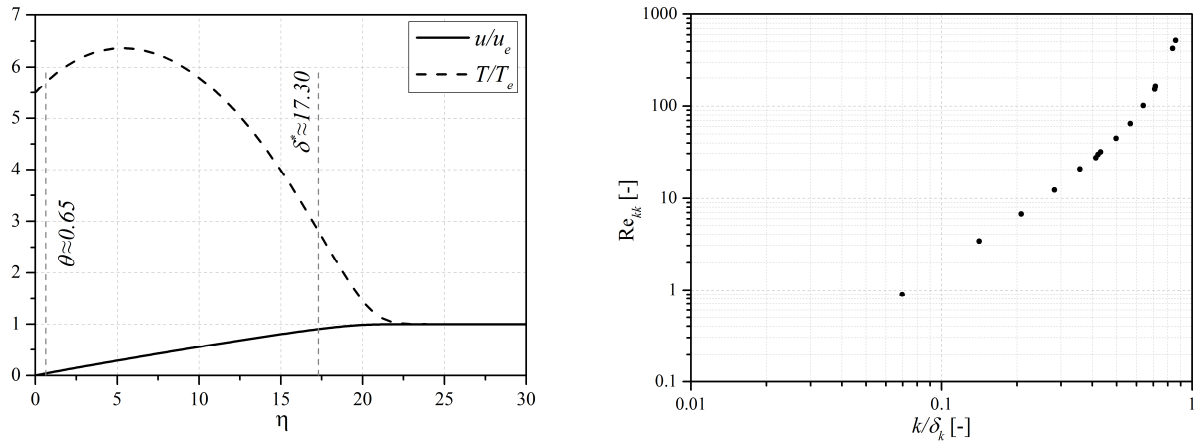

(a) (b)

Figure 8: Self-similar boundary layer profiles (a) and Re_{kk} vs. k/δ_k (b) for all experimental points under consideration. δ^* and θ stand for displacement and momentum thicknesses, respectively.

The theoretical heat flux for zero-gradient flat plate flow is calculated as follows [11]:

$$\mathrm{St}_{theory} = \frac{A}{s}\left(\frac{u_e p_e}{u_\infty p_\infty}\right)^{1-n}\left(\frac{T_\infty}{T^*}\right)^{1-2n}\left(\frac{C^*}{\mathrm{Re}_{\infty,x}}\right)^{n}, \tag{4}$$

where constants *A,s,n* and *r* are 0.332, Pr$^{2/3}$, 0.5, Pr$^{1/2}$ and 0.0296, 1, 0.2, Pr$^{1/3}$ for laminar and turbulent flows, respectively. The reference temperature T^* is computed here in accord with [12] which is a more accurate modification of the classical definition given above:

$$\frac{T^*}{T_e} = \begin{cases} 0.45 + 0.55\dfrac{T_w}{T_e} + 0.16r\dfrac{\gamma-1}{2}M_e^2, \text{laminar;} \\ 0.5\left(1+\dfrac{T_w}{T_e}\right) + 0.16r\dfrac{\gamma-1}{2}M_e^2, \text{turbulent.} \end{cases}, \tag{5}$$

The local values u_e, p_e, T_e at the edge of the boundary layer over the wedge are determined using a two-tier inviscid relation above the separation bubble, i.e. including flow deflection on the separation shock (inclined at approx. 12.5° to the plate in accord with Schlieren images for laminar separation) and the subsequent deflection to along the wedge surface. The virtual origin of two theoretical curves on the wedge (see Fig. 6) is the reattachment point obtained from the Schlieren images for the case *k*=0.0 mm (Fig. 4a, x_{rea}≈16 mm). The third theoretical curve is for laminar flat plate at free-stream parameters on the edge of the boundary layer.

To reduce experimental distributions of St(*x,z*), we find $x_{\max}$ station at which $\mathrm{St}_{zAvg}(x)$ attains its local maximum near the reattachment. Next, St($x_{\max}$,*z*) is analyzed to find its min/max and standard deviation from the mean level:

$$rms \equiv rms\left(x_{\max}\right) = \sqrt{\frac{1}{N_i}\sum_{i=1}^{N_i}\left[\mathrm{St}\left(x_{\max}, z_k\right) - St_{zAvg}\left(x_{\max}\right)\right]}, \tag{6}$$

DOI: 10.13009/EUCASS2019-200

where N_i is the number of pixels in spanwise direction of TSP image. The distribution of $St_{max} = St_{zAvg}(x_{max})$ versus k/δ_k is then subjected to nonlinear fitting with logistic curve:

$$f(x) = A_1 + \frac{A_2 - A_1}{1 + (x/x_0)^a}. \tag{7}$$

To process experimental data an interactive software has been developed using Python programming language and scientific libraries Qt5, numpy, scipy, etc.

3.4 Heating at reattachment

Consider distributions of $St_{max}(k/\delta_k)$ plotted in Fig. 9a. Keep in mind that all experiments have been performed for close Reynolds numbers and the roughness station remains unchanged. Thus, the value of boundary layer thickness changes marginally from run to run: $\delta_k = 1.42 \pm 0.02$ mm, and k/δ_k varies nearly linearly with k.

At low roughness heights, $k/\delta_k < 0.2$, the St_{max} does not appears to respond to the presence of roughness rake. Surface distributions of St remain close in amplitude with no roughness case (see Fig. 5a). At some critical value $(k/\delta_k)_{cr} \approx 0.2$ the value of St_{max} starts increasing. $St(x,z)$ field begins bearing the imprint of the roughness rake at the next closest point $k/\delta_k \approx 0.28$. Accounting for the presence of natural streamwise vortices, this behavior could mean that natural disturbances are stronger than those seeded by the roughness rake of $k/\delta_k < (k/\delta_k)_{cr} \approx 0.2$.

To support the above discussion on natural vortices, numerical simulations of two-dimensional compression corner flows are conducted in laminar and turbulent (Spalart–Allmaras closure) formulations using the in-house software HSFlow [13]. Formulation of the numerical problem is omitted for brevity. Note that turbulent simulation gives a very small separation bubble, with separation/reattachment shocks being inclined quite differently from those for laminar flow case. The corresponding levels of St are plotted in Figure 9 for reference. Note that the z-averaged experimental data sit above the computed laminar level $St_{max,cfd,lam} \approx 3.1 \times 10^{-3}$ even in the absence of the seeding roughness rake. The minimum level of $St(x_{max}, z)$ is quite close to $St_{max,cfd,lam}$. This could mean that even natural vortices are able to raise the average level of heat flux above the laminar, which may cause difficulties when comparing numerical and experimental results for this type of flows. However, the possible role of transition process cannot yet be excluded from this discussion. Thus, the conclusion drawn should be confirmed more strictly based on more evidence for laminar state of the reattachment flow, which is the matter of future effort.

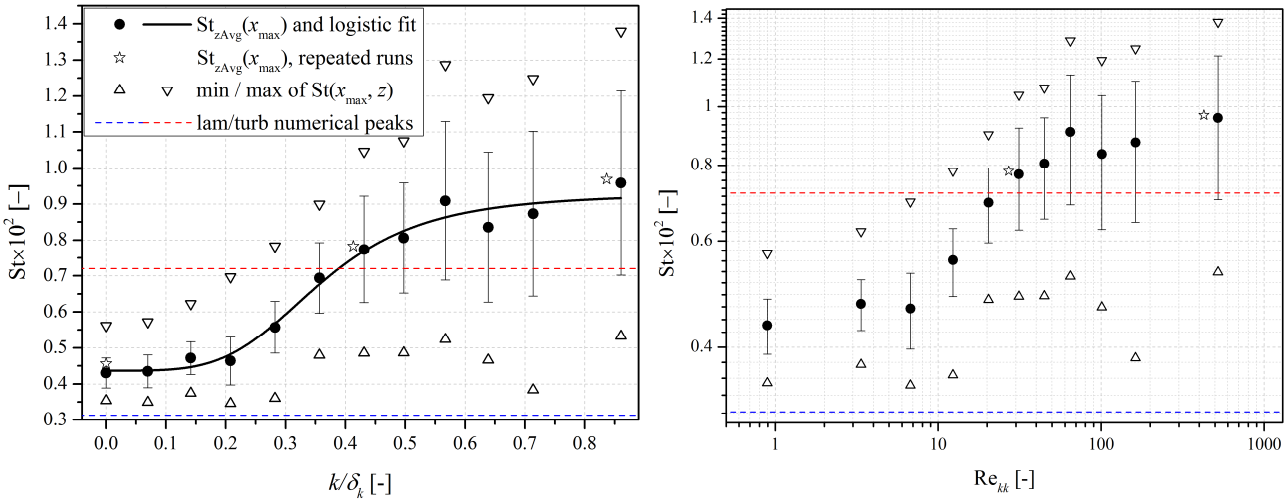

Figure 9: Dependence of maximum spanwise-averaged St number and corresponding spanwise variation of St due to vortices versus k/δ_k (a) and Re_{kk} (b). Error bars denote standard spanwise deviation, as Eq. (6).

The z-averaged maximums can be fitted using a logistic curve (see Eq. (7)) with the following coefficients (A_1; A_2; x_0;a) = (0.00929; 0.00437; 0.361; 4.13) and corresponding deviations (3.4×10^{-4}; 2.1×10^{-4}; 0.022; 0.97). It suggests that the rising trend saturates for large roughness elements, which might correspond to the fact that the roughness elements

DOI: 10.13009/EUCASS2019-200

are located rather close to each other and begin working like a solid 2D spanwise roughness strip when the height k becomes large. The spacing-to-diameter ratio of roughness elements is two, which makes this suggestion possible [5].

Despite the saturation of St_{max}, the spanwise deviation of St at station x_{max}, *rms* of Eq. (6), does not saturate (see Fig. 10) as k/δ_k rises. They are nearly constant for $k/\delta_k<(k/\delta_k)_{cr}$ and start increasing nearly linearly for approx. $k/\delta_k>(k/\delta_k)_{cr.}$ Extension of the regression line over the rising portion of data to lower values of k/δ_k comes very close to zero. This supports two statements: 1) spanwise rms variation of St due to vortices is linearly dependent on the height of the seeding roughness rake, with no variation at no roughness (linear receptivity of boundary layer to the roughness rake); 2) natural level of disturbances that turn into Goertler vortices at reattachment correspond to the roughness of the critical height.

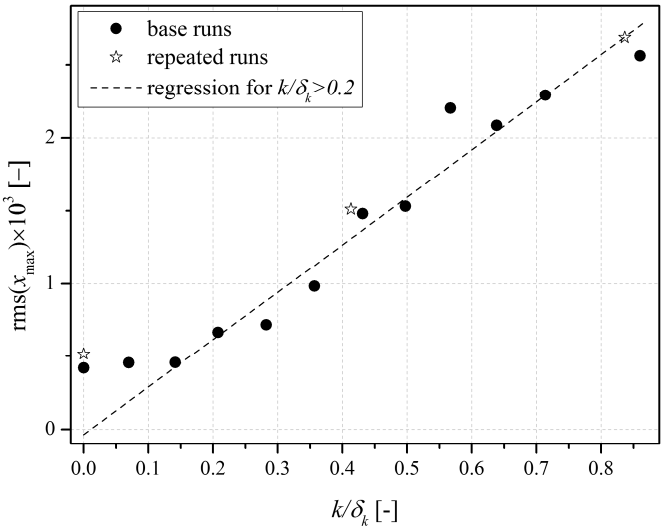

Figure 10: Dependence of St variations due to vortices on k/δ_k. Linear regression: $f(k/\delta_k) = (325.7k/\delta_k + 3.6)\times10^{-5}$.

4. Conclusion

Experimental investigation of the effect of Goertler-type vortices on heat transfer in nominally two-dimensional compression corner flow has been carried out at Mach 8, Reynolds number based on the flat plate length $(1.75\pm0.09)\times10^5$ and wall-to-stagnation temperature ratio 0.40. The experiments include Schlieren imaging and TSP measurements. The vortices have been induced naturally (by themselves) or artificially by using a rake of cylindrical roughness elements of heights from 0.1 to 1.2 mm, diameter 1.7 mm and spacing 3.4 mm. The state of boundary layer at reattachment is close to laminar.

The vortices are capable of increasing the spanwise-averaged heat flux behind the reattachment region independent on weather the boundary layer is laminar or transitional. This effect may confuse the comparison of numerical and experimental results. The effect saturates as the roughness height reaches the value of the boundary layer thickness. Spanwise rms variation of heat transfer coefficient increases linearly with roughness height, with no variation at no roughness, which points to nearly linear receptivity of the boundary layer to the height of the roughness rake elements.

Acknowledgments

The work has been supported by Russian foundation for basic research (project no. 17-08-00567 for experiments, processing and analysis; project no. 18-38-20091 for extended version of boundary layer solver).

References

[1] Chuvakhov, P. V., Borovoy, V. Ya., Egorov, I. V., Radchenko, V. N., Olivier, H. and A. Roghelia. 2017. Effect of Small Bluntness on Formation of Görtler Vortices in a Supersonic Compression Corner Flow. *Journal of Applied Mechanics and Technical Physics* 58(6):975–989.

[2] Simeonides, G. and W. Haase. 1995. Experimental and Computational Investigations of Hypersonic Flow about Compression Ramps. *J. Fluid Mech.* 283(1) :17–42.

DOI: 10.13009/EUCASS2019-200

[3] Chuvakhov, P. V., Egorov, I. V., Olivier, H. and A. Roghelia. 2016. Joint Influence of High Entropy Layer and Goertler Vortices on Heat Transfer in Supersonic Compression Ramp Flow. *Computational Thermal Sciences: An International Journal* 8(6):543–553.
[4] Sivasubramanian, J. and H. F. Fasel. 2015. Direct Numerical Simulation of Transition in a sharp cone boundary layer at Mach 6: fundamental breakdown. *J. Fluid Mech.* 768 :175–218.
[5] Schneider, S. P. 2008. Effects of Roughness on Hypersonic Boundary-Layer Transition. *Journal of Spacecraft and Rockets* 45(2):193–209.
[6] Hung, F. and D. Barnett. 1973. Shockwave-boundary layer interference heating analysis. *AIAA Paper* No. 73–237.
[7] Borovoy, V. Ya., Mosharov, V. E., Noev A. Yu. and V. N. Radchenko. 2009. Laminar-turbulent flow over wedges mounted on sharp and blunt plates. *Fluid Dynamics* 44(3):382–396.
[8] Candler, G. V. 2011. Numerical simulation of hypersonic shock wave–boundary-layer interactions. In: *Shock wave–boundary-layer interactions* by H. Babinsky and J. K. Harvey (eds.), 1st edition, Cambridge University Press, pp. 314–335.
[9] Roghelia, A., Olivier, H., Egorov, I. and P. Chuvakhov. 2017. Experimental investigation of Görtler vortices in hypersonic ramp flows. *Exp Fluids* 58:139.
[10] Ginoux, J. J. 1978. Laminar Boundary Layers. Course note 104. Von Karman Institute for Fluid Dynamics, Rhode-Saint-Genèse.
[11] Simeonides, G. 1992. Hypersonic shock wave boundary layer interactions over compression corners. PhD Thesis. University of Bristol.
[12] Meador, W. E. and M. K. Smart. 2005. Reference enthalpy method developed from solutions of the boundary-layer equations. *AIAA J* 43:135–139.
[13] Egorov, I. V. and A. V. Novikov. 2016. Direct numerical simulation of laminar–turbulent flow over a flat plate at hypersonic flow speeds. *Computational Mathematics and Mathematical Physics* 56(6):1048–1064.